The Journal of Chemical Physics

Effect of isotope substitution on the Fermi resonance and vibrational lifetime of unnatural amino acids modified with IR probe: A 2D-IR and pump-probe study of 4-azido-L-phenyl alanine

Cite as: J. Chem. Phys. **153**, 164309 (2020); https://doi.org/10.1063/5.0025289
Submitted: 14 August 2020 . Accepted: 12 October 2020 . Published Online: 28 October 2020

Jun Young Park, Saptarsi Mondal, Hyeok-Jun Kwon, Prabhat Kumar Sahu, Hogyu Han, Kyungwon Kwak, and Minhaeng Cho

AIP Publishing

The Journal of Chemical Physics ARTICLE scitation.org/journal/jcp

Effect of isotope substitution on the Fermi resonance and vibrational lifetime of unnatural amino acids modified with IR probe: A 2D-IR and pump-probe study of 4-azido-L-phenyl alanine

Cite as: J. Chem. Phys. 153, 164309 (2020); doi: 10.1063/5.0025289
Submitted: 14 August 2020 • Accepted: 12 October 2020 •
Published Online: 28 October 2020

Jun Young Park,[1,2] Saptarsi Mondal,[1,2] Hyeok-Jun Kwon,[2] Prabhat Kumar Sahu,[1,2] Hogyu Han,[2,a)] Kyungwon Kwak,[1,2,a)] and Minhaeng Cho[1,2,a)]

AFFILIATIONS

[1]Center for Molecular Spectroscopy and Dynamics, Institute for Basic Science (IBS), Korea University, Seoul 02841, South Korea
[2]Department of Chemistry, Korea University, Seoul 02841, South Korea

[a)]**Authors to whom correspondence should be addressed:** hogyuhan@korea.ac.kr; kkwak@korea.ac.kr; and mcho@korea.ac.kr

ABSTRACT

The infrared (IR) probe often suffers from an unexpected complex absorption profile due to the Fermi resonance and short vibrational lifetime, which restricts the application of time-resolved IR spectroscopy to investigate the site-specific structural dynamics of the protein. Researchers have found that isotope substitution to the IR probe not only removes the Fermi resonance but also extends the dynamic observation window with a prolonged vibrational lifetime. This method has been successfully applied to modify the vibrational properties of many IR probes for time-resolved spectroscopy and imaging. In this study, the effect of isotope substitution (^{15}N) on the vibrational properties of the azide stretching band in 4-azido-L-phenylalanine has been investigated using ultrafast pump-probe and 2D-IR spectroscopy. In contrast to the earlier reports, it has been observed that the Fermi resonance remains unchanged even after isotope substitution, and there is very little change in the vibrational relaxation dynamics as well. Anharmonic frequency analysis reveals that the α-N atom of N_3 is being shared between the two transitions participating in the Fermi resonance and gets affected similarly due to isotope labeling. Hence, this study unveils the specific circumstance at which the isotope labeling strategy may not be successful in eliminating the Fermi resonance band and explains the molecular origin behind it. This study also suggests definitive approaches on how to overcome the limitations related to the Fermi resonance to extend the development and application of this IR probe for biological research.

I. INTRODUCTION

Understanding the interplay between the structure, dynamics, and function of the biomolecule using ultrafast vibrational spectroscopy requires site-specific intervention to get an in-depth molecular-level picture by attaching a reporter extremely sensitive to the local environment.[1–7] Infrared (IR) probes are the most suitable candidate to be used as a site-specific marker because of their high sensitivity to the local environment, high selectivity from the site-specific insertion of unnatural amino acids modified with the IR probe into proteins, and minimal perturbation to the native structure owing to its tiny size constituting of two or three atoms.[1,2,8–13] Spectroscopic methods like 2D-IR comprising these site-specific infrared probes can elucidate the microscopic structure and dynamics of the biomolecules in great detail.[14–21] Indeed, 2D-IR spectroscopy has been implemented to investigate the protein folding dynamics, amyloid aggregates, chemical exchange processes, hydrogen bond dynamics, solute–solvent interaction, and protein

recognition in combination with the site-specific infrared probes such as carbonyl (CO), cyano (CN), thiocyano (SCN), and azide (N_3) groups.[1,3–7,11,12,16,18,20–39] Therefore, extensive research has been carried out to develop new infrared probes that (a) have an intense infrared band with narrow spectral bandwidth and (b) fall in the transparent window (1800 cm^{-1}–2500 cm^{-1}), and hence get separated from the water and protein vibration, which do not usually appear in that region.[1,11–13]

Though there are significant advantages of using these infrared probes in vibrational spectroscopy and microscopy, there are some disadvantages too. The infrared probe often suffers from a short vibrational lifetime and complex absorptive line shape due to the Fermi resonance between a fundamental band and a near-resonant overtone/combination band.[40–42] Therefore, it is necessary to develop new IR probes having a longer vibrational lifetime to investigate the dynamics essential to the function of the biomolecule, which may occur on a longer time scale. On the other hand, the presence of the Fermi resonance results in an asymmetric broadening of the absorption band with a shoulder peak, which makes the spectroscopic analyses of FT-IR, pump-probe, and especially 2D-IR spectra very difficult due to the band overlap.[21,30,40–43]

The incorporation of the heavy atom in the infrared probe was proposed to increase the vibrational lifetime of the probe, and further studies have revealed that the heavy atom could also increase the signal intensity of the IR probe, significantly.[26,28,44,45] The incorporation of the heavy atom between the probe group and the main biological molecule disconnects the vibrational coupling between the donor and acceptor modes of vibrational excitation. Consequently, the vibrational lifetime gets increased due to the removal of the fast relaxation pathways. For example, it has been shown that the incorporation of Se in the CN probe can increase the vibrational lifetime by 3–4 times (170 ps–330 ps), as compared to the SCN group.[44]

In comparison to the heavy atom insertion technique where the electronic potential of the probe molecule gets changed along with the molecular geometry, isotope substitution ensures that there is a minimal perturbation in the native structure of the protein. Additionally, isotope substitution inherently manipulates the energy levels of the vibrational states. Therefore, it can efficiently decouple the participating bands in the Fermi resonance or restrict other non-radiative decay channels but do not interfere with the molecular structure. Consequently, the vibrational lifetime gets enhanced.[27,29–32,46] For example, Le Sueur *et al.* have shown that the ^{13}C and ^{15}N substitution in CN-phenylalanine increases the time window of 2D-IR spectroscopic measurement by twofold.[46] It has been demonstrated that the spectral shifts can also be effectively modulated to meet different needs in the experiment.[27,29,30,46] Since the electric potential of the molecule of interest is not affected by the isotope substitution and, hence, its interaction with the solvent, the resultant changes can be directly correlated with the interaction among the vibrational degrees of freedom of the molecule. Therefore, the method of isotope substitution can be used to investigate the underlying vibrational relaxation mechanism. For example, the vibrational relaxation mechanism has been thoroughly studied by substituting ^{13}C and ^{15}N isotopes in the CN isotopomer in unnatural amino acids, namely, cyano-phenylalanine.[27]

Recently, unnatural amino acids comprising the azide group as an IR probe have been implemented in both spectroscopy and microscopy to understand various biological systems because of the very high molar extinction coefficient and IR absorption cross section of azides.[47–52] The molar extinction coefficient of azide larger than that of nitrile (13 times) makes it a very useful and cost-effective IR probe for the tagged protein preparation. A strong signal of the azide allows the study of a very low concentrated solution of the protein, removing the possibility of protein–protein aggregation in the solution. This makes the azide a highly attractive IR probe for studying biological systems. Recently, Shi *et al.* have employed azidohomoalanine as an IR tag to investigate *in vivo* mid-IR metabolic imaging at tissues and organs.[53] However, this promising probe shows a complex absorption profile in FT-IR and 2D-IR, which restricts its broader applicability in the biological research. Therefore, it is essential to perform an in-depth spectroscopic analysis of this probe to modulate its vibrational properties.

Recent time-resolved studies of 4-azido-L-phenylalanine have been performed in polar protic solvents to replicate the biological environment and understand its impact on the vibrational properties.[40] However, the presence of hydrogen bonding does complicate the spectra analysis and its interpretation. Therefore, in this study, all the experiments have been performed in aprotic solvent dimethylformamide (DMF) to focus more on the vibrational properties of the probe itself rather than the environmental effects. To achieve this goal, L-phenylalanine is modified to synthesize the 4-azido-L-phenylalanine derivative (Ac-p-N_3-Phe-OMe, Fig. 1) that mimics azide-labeled proteins. From here, we call the 4-azido-L-phenylalanine derivative as aromatic azide only because it is enough to represent the spectroscopic features of the IR probe. Isotope substitution has been successfully applied in the azide to get rid of the accidental Fermi resonances. Lipkin *et al.* have shown that the ^{15}N isotope substitution in the beta position of the azide in Pyr$N^{15}NN$ can remove the Fermi resonance.[30] Therefore, we have also employed the isotope substitution (^{15}N) in the mid-N atom of the azide group of the aromatic azide and report how it affects the vibrational band profile and relaxation dynamics of the azide probe. Additionally, we have also tested whether the coupling constant associated with the Fermi resonance in the azide system can be equally sensitive to the solvent polarity and hydrogen bonding environment, as previously proposed by Rodgers *et al.* for –CO and –CN infrared probes.[41] In summary, the present investigation reveals specific circumstances where the isotope substitution strategy might not work as expected and describes the molecular origin behind it.

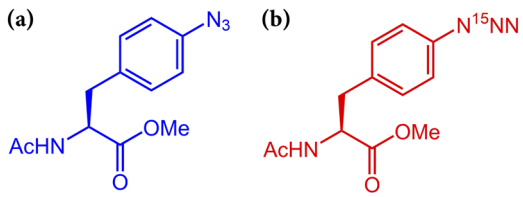

FIG. 1. Structure of the (a) unlabeled aromatic azide (Ac-p-N_3-Phe-OMe) and (b) labeled aromatic azide (Ac-p-$N^{15}NN$-Phe-OMe) in its L-form.

II. MATERIALS AND METHODS

A. Materials

The unlabeled and labeled azide derivatives exclusively in its L-form [Figs. 1(a) and 1(b)] were synthesized, and the corresponding proton nuclear magnetic resonance (1H NMR, 500 MHz) data in CDCl3 can be found in the supplementary material. Purified water (H_2O, Millipore, 18.2 MΩ cm resistivity) was used for the measurement, whereas spectroscopy grade dimethylformamide (DMF) and D_2O were purchased from Sigma-Aldrich and used without further purification.

B. Methods

1. FT-IR spectroscopy

The steady-state spectra of the unlabeled and labeled aromatic azide were measured in DMF using a Bruker Vertex 70 FT-IR spectrometer with a HgCdTe (MCT) detector filled with liquid nitrogen (N_2, Billerica, MA). The frequency resolution of the spectrometer was set to 1 cm^{-1}. All measurements were performed using a homemade liquid cell, which consists of two CaF_2 windows of 2 mm thickness. The cell path length was set to be 25 μm using a Teflon spacer.

2. Ultrafast IR pump-probe spectroscopy

A spitfire regenerative amplifier (Spectra-Physics, Inc.; Santa Clara, CA) was used to generate an output of 1 W power and a repetition rate of 1 kHz centered around 800 nm, which was used as the gate pulse for the homemade optical parametric amplifier (OPA). A 6.6 W DPSS laser (Millennia, Spectra-Physics) was used to pump the regenerative amplifier, whereas a Ti:sapphire oscillator (Tsunami) was used as a seed laser. The output from the OPA with a 1 kHz repetition rate consisting of both the signal and idler beams was used to produce the mid-IR pulse from an $AgGaS_2$ nonlinear crystal using the difference frequency generation technique. A beam splitter was used to separate the primary mid-IR signal with the intensity ratio of 9:1 for the pump and probe beam, respectively. A motorized linear delay stage was used in the probe beamline to control the delay time in the time-domain measurement. A 32-element MCT array detector with a resolution of 2 cm^{-1}/pixel was used to collect and analyze the dispersed pump-probe signal from a monochromator. The relative polarization of the probe beam was controlled using a rotating polarizer. To calculate the isotropic relaxation dynamics, we measured the population relaxation decay at two different polarization conditions for the probe and pump beams, i.e., at the parallel ($S_\parallel$) and perpendicular ($S_\perp$) position. We used a homemade cell of 25 μm path length consisting of two CaF_2 windows of 2 mm thickness and a Teflon spacer. Population relaxation, P(t) (vibrational lifetime), was calculated using the following equation:

$$P(t) = \frac{S_\parallel + 2S_\perp}{3}. \quad (1)$$

3. 2D-IR vibrational echo spectroscopy

The detailed description of the 2D-IR vibrational spectroscopy has been discussed elsewhere.[22] Shortly, a mid-IR pulse centered at 2110 cm^{-1} or 2060 cm^{-1} was split into three pulses of approximately the same power. These three pulsed beams were focused onto the sample in BoxCARS geometry. The IR pulse 3 (k_3) was fixed in time and chopped at 500 Hz. In 2D-IR vibrational echo spectroscopy, the temporal overlap of the three pulses leads to the generation of a third-order echo signal in the phase-matched direction ($-k_1 + k_2 + k_3$). This signal was heterodyne detected by overlapping with a local oscillator pulse. A monochromator dispersed the combined beam onto a 32-element MCT array detector (~2 cm^{-1}/pixel resolution). We denoted the delay times between the pulses 1 and 2, and between the pulses 2 and 3, as τ and T_w, respectively. The 2D-IR spectra were obtained as a function of T_w.

4. Quantum chemical calculation

All quantum chemical calculations were carried out using the Gaussian 16 quantum chemistry package.[54] Geometry optimizations were performed using the B3LYP/6-311++G and B3LYP/6-311+G** level of theory. Frozen core approximation and very tight convergence criteria were employed during geometry optimization. The absence of any negative frequency indicates that the calculated geometries are at local minima. We used the conductor-like polarizable continuum model (CPCM) for dimethylformamide (DMF) to include the effect of the solvent in the calculation.

Anharmonic frequencies were computed at the B3LYP/6-311+G** level of theory using the CPCM solvation model. To find out the most suitable interactions to be considered as Fermi resonance, we used the following criteria: the maximum frequency range of ±25.0 cm^{-1} from the azide asymmetric stretch was considered; the minimum cubic force constant (the third derivative of energy, $|k_{ijk}|$) is 1 cm^{-1}; the minimum difference of the second-order perturbative energy (PT2) to the variational energy is 1 cm^{-1}.[40,55]

III. RESULTS AND DISCUSSION

A. FT-IR spectroscopy of the azide probes

The FT-IR spectra of the unlabeled and labeled aromatic azide in the DMF solvent are shown in Fig. 2. Both the unlabeled and labeled azides [Figs. 2(a) and 2(b)] show a complex azide stretching band profile that is deconvoluted using two Voigt functions. The fitting parameters in both cases are listed in Table I. The unlabeled azide shows an intense peak at 2118 cm^{-1} and a shoulder peak around 2084 cm^{-1}. The ratio of the integrated area under the main peak to that of the shoulder peak is around 4.4:1, and the corresponding full width at half maxima (FWHM) is found to be 27.3 cm^{-1} and 37.5 cm^{-1}, respectively. Upon isotope substitution, the azide stretch shifts to the lower frequency by 52 cm^{-1} (redshift). However, it also shows the complex absorption band profile with the main peak appearing at 2066 cm^{-1} and a shoulder peak at around 2099 cm^{-1}. The ratio of the integrated area of the main peak to that of the shoulder peak is 5.9:1, and the corresponding FWHMs are 24.9 cm^{-1} and 32.7 cm^{-1}. The presence of the shoulder peak in both cases indicates the presence of either a different conformer or Fermi resonance band between the azide asymmetric stretch mode and other near-resonant bands. The higher FWHM of the Fermi resonance band than the azide asymmetric stretch band for both the unlabeled and labeled azide suggests that the Fermi resonance band is slightly more affected by inhomogeneous broadening. Interestingly, we observe that the shoulder peak shows a blue-shift

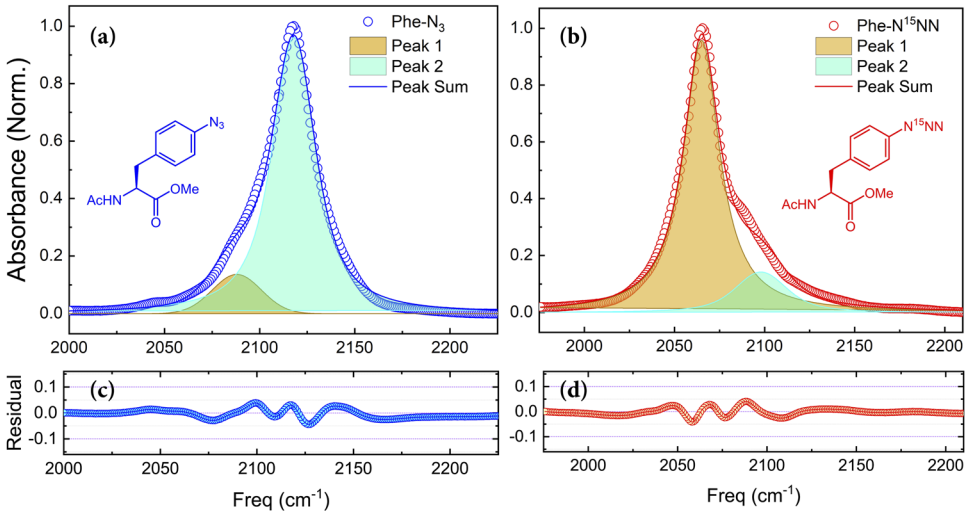

FIG. 2. Steady-state FT-IR spectra with spectral deconvolution using two Voigt functions of (a) unlabeled and (b) ^{15}N labeled aromatic azides at the β position in the DMF solvent. The residual of fitting is shown in the bottom panel for the unlabeled azide (c) and labeled azide (d).

(15.0 cm^{-1}) along with the expected red-shift in the azide asymmetric stretch upon isotope substitution. The presence of the shoulder peak in both unsubstituted and substituted aromatic azides shows that isotope labeling does not help simplify the complex absorption band profile of the N_3 asymmetric stretch band.

B. 2D-IR spectroscopy of azide probes

To ensure whether the two observed bands in the FT-IR spectra arise from the Fermi resonance coupling or two different conformations, we have measured the 2D-IR spectra of the aromatic azide. 2D-IR spectroscopy has been implemented before to characterize the relationships between the vibrational modes observed in steady-state FT-IR spectra. The Fermi resonance appears in the 2D-IR spectrum as a cross-peak at an early waiting time (T_w), whereas, for chemical exchange processes between two conformers, the cross-peak starts to appear at a later waiting time and gradually evolves with the increase of waiting time. We have shown the 2D-IR vibrational echo spectra of both unlabeled and labeled aromatic azides in Fig. 3 at zero waiting time (T_w = 0 ps). In Fig. 3, ω_τ and ω_m refer to the pump and probe frequency in the measurement, respectively. The vibrational transitions corresponding to the ground-state bleach and the stimulated emission (SE) combined appear as a positive peak (red).

TABLE I. Fitting results for FT-IR spectra of azide derivatives using the Voigt function in the DMF solvent. The peak frequencies (ω_0) and FWHM are in cm^{-1}. The area represents the relative area of the main peak to the shoulder peak.

	Peak 1			Peak 2		
System	ω_0	FWHM	Area	ω_0	FWHM	Area
Phe-N_3	2084.0	37.5	1.0	2118.0	27.3	4.4
Phe-N^{15}NN	2066.0	24.9	5.9	2099.0	32.7	1.0

In contrast, the excited-state absorption appears as a negative peak (blue) in a typical 2D-IR spectrum, as shown in Fig. 3. In the case of unlabeled azide [Fig. 3(a)], there is only one distinct positive peak at (ω_τ, ω_m) = (2118, 2118) cm^{-1} corresponding to the 0–1 transition along with the associated negative peak at (ω_τ, ω_m) = (2118, 2066) cm^{-1} for the 1–2 transition. However, the shoulder peak around 2084 cm^{-1}, as observed in the FT-IR spectra, is not clearly identifiable as a separate peak along the diagonal line in the 2D-IR spectrum. A similar spectral feature can be seen in the case of labeled azide [Fig. 3(b)] as well, where the positive peak corresponding to the 0–1 transition is at 2066 cm^{-1} on the diagonal, and the corresponding negative peak for the 1–2 transition can be traced at (ω_τ, ω_m) = (2066, 2034) cm^{-1}. At the same time, there is no distinct positive peak along the diagonal around (ω_τ, ω_m) = (2099, 2099) cm^{-1} corresponding to the shoulder peak, as observed in the FT-IR spectra of the labeled aromatic azide.

However, there is elongation in the off-diagonal direction toward left from the strongest peak at 2118 cm^{-1} for the unlabeled azide. Similarly, there is also off-diagonal elongation into the top and right side of the positive diagonal peak at 2066 cm^{-1} in the case of the labeled azide. In one of the previous studies of 4-azido-L-phenylalanine (pN_3Phe) dissolved in a protic solvent, Zhang *et al.* have analyzed and identified such types of off-diagonal distortions as cross-peaks that arise from the Fermi resonance coupling.[40] The absence of the diagonal-peak (shoulder peak in the FT-IR) in the 2D-IR spectra of both the unlabeled and labeled azides can be understood based on the sensitivity of the 2D-IR signal and the transition dipole moment (μ) associated with the corresponding vibrational transition. The spectral intensity in the case of 2D-IR is proportional to $|\mu|^4$ compared to $|\mu|^2$ in the FT-IR spectra. Thus, any small changes in μ get magnified in 2D-IR, making the strong signal stronger and the weak signal weaker.[16] This high contrast scenario makes the weak signal hard to intercept in the 2D-IR spectra. Therefore, our study suggests that the transition dipole strength of the azide peak is much higher than that of the shoulder peak in the 2D-IR spectra even though the near-resonant band gets a portion of the

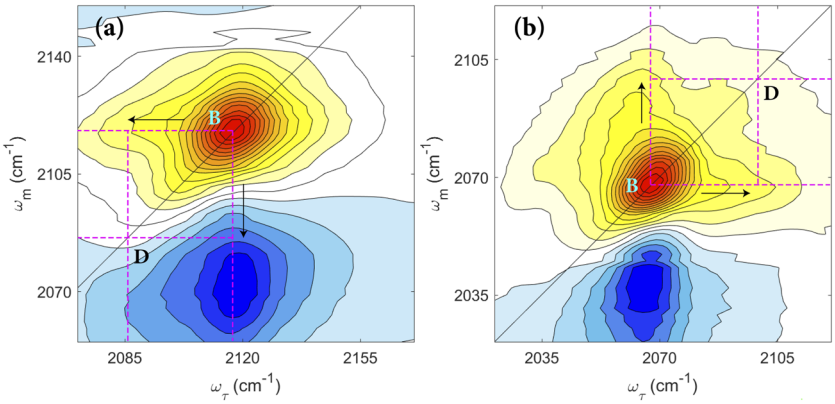

FIG. 3. 2D-IR vibrational echo spectra for azide derivatives at zero waiting time (T_w = 0 ps) of the unlabeled aromatic azide (a) and labeled aromatic azide (b). B (cyan) and D (black) in the spectra represent a bright state (high intensity) and a dark state (very low intensity), respectively.

oscillator strength from the azide fundamental transition band due to intensity redistribution through the Fermi resonance.

According to that analogy, it has been observed that the two positive peaks appear on the diagonal at (ω_τ, ω_m) = (2084, 2084) cm^{-1} and (ω_τ, ω_m) = (2118, 2118) cm^{-1} for the unlabeled azide, but the peak at (ω_τ, ω_m) = (2084, 2084) cm^{-1} does not appear as a separate peak because of the weak transition dipole moment, which almost fades away in 2D-IR. The cross-peak arising from the Fermi resonance coupling between the two participating modes appears at (ω_τ, ω_m) = (2084, 2118) cm^{-1}. In contrast, the other cross-peak at (ω_τ, ω_m) = (2118, 2084) cm^{-1} does not show up because of its destructive overlap with the 1–2 transition at that position. Similarly, in the case of the labeled azide, the cross-peaks come at (ω_τ, ω_m) = (2066, 2099) cm^{-1} and (ω_τ, ω_m) = (2099, 2066) cm^{-1} arising from the Fermi resonance. The diagonal slice of the 2D-IR spectra of PheN$_3$ and PheN^{15}NN is plotted in Fig. S6 of the supplementary material. The asymmetric broadening of the diagonal slice of 2D-IR in the low-frequency region in the case of PhN$_3$ and a clear shoulder peak at the high-frequency region for the labeled azide PhN^{15}NN indicates the existence of the Fermi resonance band. However, the shoulder peak is difficult to observe in the case PheN$_3$ because of the overlap of the 0–1 transition with the 1–2 transition, which reduces the signal intensity. Thus, the 2D-IR spectra prove that the shoulder peak observed in the steady-state FT-IR spectra at 2066 cm^{-1} for the unlabeled azide and 2099 cm^{-1} for the labeled azide is due to the Fermi resonance, which shows that the isotope substitution could not remove the Fermi resonance from the aromatic azide, despite the substantial spectral shift of 52 cm^{-1} of the azide asymmetric stretch due to isotope substitution.

C. IR pump-probe spectroscopies of azide probes

We have measured the vibrational lifetime of the azide probe using polarization-controlled IR pump-probe experiments to determine how isotope labeling affects the vibrational relaxation dynamics of the azide probe. In a typical pump-probe spectrum, a positive peak (0–1 transition) corresponding to the ground state bleach (GSB) and stimulated emission (SE) appears at a higher frequency, whereas the negative peak (1–2 transition) arising from the excited state absorption (ESA) process of the probe molecule shows up at a lower frequency. In Fig. 4, we have shown the pump-probe decay profiles of the 1–2 transitions for both the unlabeled (red) and labeled (blue) aromatic azides to avoid possible pump-induced local heating contribution, which is more significant in the 0–1 transitions. The excited-state decay traces show an oscillatory beating feature for both the unlabeled and labeled azides. The presence of the oscillatory beating feature is the salient characteristic of the Fermi resonance in the system, as reported previously.[40–42] Therefore, we have fitted both the unlabeled and labeled azides using one exponential function and one damped oscillation function (described in Table II). Table II summarizes the fitting results for the vibrational dynamics corresponding to 1–2 transitions for both the unlabeled and labeled azides. The period (T) of the oscillations of the

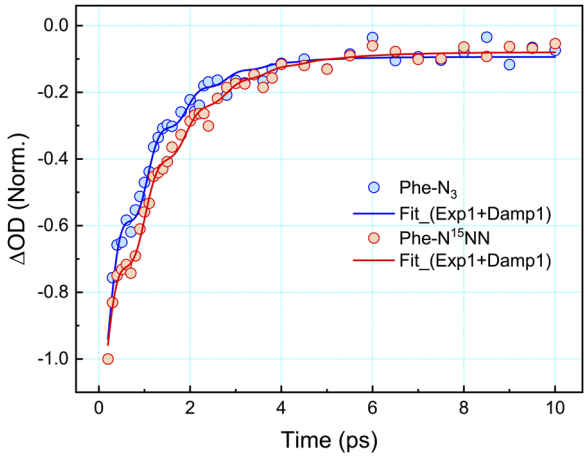

FIG. 4. Vibrational relaxation dynamics corresponding to the 1–2 transition of unlabeled (blue circles) and labeled (red circles) aromatic azides in the DMF solvent. The solid red and blue lines show the fitting of the vibrational relaxation dynamics of the respective azides using a single exponential and a damped function. Selected probe frequencies at which the population relaxation has been shown are 2077 cm^{-1} and 2039 cm^{-1} for unlabeled and labeled aromatic azides, respectively. The presence of the oscillatory decay pattern in the vibrational dynamics is the salient characteristic of the existence of the Fermi resonance in the azide system.

TABLE II. The fitting parameters of the vibrational dynamics of unlabeled (Phe-N_3) and labeled (Phe-$N^{15}NN$) aromatic azides using an exponential and a damped oscillation function as follows: $y = y_0 + A_1 e^{-x/\tau_1} + A_2 e^{-x/\tau_2} \cos\left(\frac{2\pi x}{T} - \Phi\right)$. $a_1 = A_1/A_1 + A_2$ and $a_2 = 1 - a_1$ represent the normalized preexponential factors associated with the t_1 and t_2 lifetime components, respectively. T and $\tilde{\nu}$ represent the time period of the oscillation and the energy gap associated with the corresponding 1–2 transitions in the unlabeled and labeled azides, respectively. The standard errors have been listed along with the respective parameters wherever it can be derived.

System	τ_1 (ps)	a_1	τ_2 (ps)	a_2	Φ	T (ps)	$\tilde{\nu}$ (cm^{-1})
Phe-N_3	1.02 ± 0.05	−0.88 ± 0.03	0.90 ± 0.04	−0.12 ± 0.03	0.33 ± 0.05	0.87 ± 0.05	38.3
Phe-$N^{15}NN$	1.29 ± 0.04	−0.91 ± 0.02	1.00 ± 0.04	−0.09 ± 0.02	−0.34 ± 0.05	0.90 ± 0.04	37.0

decay traces of the aromatic azide before and after isotope labeling (Table II) is found to be around 0.87 ps and 0.90 ps corresponding to 38.3 cm^{-1} and 37.0 cm^{-1}, respectively. They should be matched with the energy gaps between the states involved in the Fermi resonance and are in good agreement with the experimental result. Therefore, the oscillatory decay traces of the vibrational relaxation dynamics are assigned to the coherence excitation of the Fermi coupled states. The vibrational lifetimes corresponding to the exponential decay are 1.02 ps and 1.29 ps, respectively, for the unlabeled and labeled azides, which show the increase due to isotope substitution. Additionally, the time constants associated with the damped oscillatory decay are 0.90 ps and 1.00 ps for the unlabeled and labeled aromatic azides, respectively.

The increase of the vibrational lifetime due to isotope substitution is very marginal contrary to the earlier reports where isotope substitution has been found to increase the vibrational lifetime significantly, sometimes, twofold to threefold from the corresponding unsubstituted system.[27,29,30,46] Therefore, this study shows that the isotope substitution strategy has become unsuccessful in enhancing the vibrational lifetime of the azide molecule in this case. However, the small increase (~25%) in the vibrational lifetime can provide a clue to the vibrational relaxation pathway of the aromatic azide band. The shoulder peak participating in the Fermi resonance has been expected to be one of the major acceptor states for intramolecular vibrational energy transfer. Here, the intramolecular vibrational relaxation in the unlabeled aromatic azide is a down-hill energy transfer because the donor state (azide stretching band) is placed higher than the acceptor states (the shoulder band). In contrast, the vibrational relaxation in the isotope-labeled aromatic azide goes through a less efficient up-hill pathway because of the red-shift in the azide stretching band. The relative difference in these energy transfer processes thus accounts for an overall 25% increase of the vibrational lifetime for the labeled azide based on the energy difference between the donor and acceptor states. This observation demonstrates that the red-shift of the azide asymmetric stretch due to single isotope labeling is not enough to alter the vibrational relaxation mechanism.

D. Two-state model

To understand whether vibrational coupling corresponding to the Fermi resonance can be used as a reliable indicator of the H-bonding status in the aromatic azides, we have measured FT-IR spectra in polar protic solvents H_2O and D_2O and aprotic solvent DMF. The FT-IR spectra of the azide stretch in H_2O and D_2O are shown in Fig. S1 and Table S1 of the supplementary material and DMF in Fig. 2. We have computed the unperturbed energy levels and coupling between two vibrational modes from the FT-IR spectra using the two-state model. In this model, we assume that coupling constants in the aromatic azides are the same before and after the isotope substitution. Thus, we write zeroth-order Hamiltonian matrices of aromatic azides with and without isotope labeling as follows:

$$H_1 = \begin{pmatrix} \varepsilon_1 & \beta_{12} \\ \beta_{12} & \varepsilon_2 \end{pmatrix}, \tag{2}$$

$$H_2 = \begin{pmatrix} \varepsilon_1 - \Delta & \beta_{12} \\ \beta_{12} & \varepsilon_2^* \end{pmatrix}, \tag{3}$$

where H_1 represents the Hamiltonian for the aromatic azide without isotope labeling, H_2 corresponds to the aromatic azide with isotope labeling, ε_1, ε_2, and ε_2^* represent the zeroth-order energy states, and β_{12} indicates the coupling strength between zeroth-order energy states. Here, we expect that isotope labeling may cause a shift in the overtone or combination band (ε_2); hence, we denote the shifted frequency as ε_2^*. The frequency shift (Δ) due to reduced mass effect from isotope labeling has been computed using the quantum chemical calculation (discussed in Sec. III E) and found to be ~44 cm^{-1} without Fermi resonance. We have calculated the characteristic polynomial of H_1 and H_2 according to the following equation:

$$P_{H_n}(\lambda_n) = |H_n - \lambda_n I| = 0. \tag{4}$$

Here, λ_n is one of the eigenvalues, and I is the unit matrix. The diagonalization of H_n generates the eigenvectors of the H_n matrix (A_n) and eigenvalues (Λ_n), whose elements are the frequencies obtained from the FT-IR spectra of aromatic azides in DMF,

$$\Lambda_1 = \begin{pmatrix} 2118 & 0 \\ 0 & 2084 \end{pmatrix}, \tag{5}$$

$$\Lambda_2 = \begin{pmatrix} 2066 & 0 \\ 0 & 2099 \end{pmatrix}. \tag{6}$$

H_n can be rewritten as $H_n = A_n \Lambda_n A_n^{\dagger}$. We have solved these equations and depict the result in Fig. 5. The result shows the zeroth-order energy states of the aromatic azide.

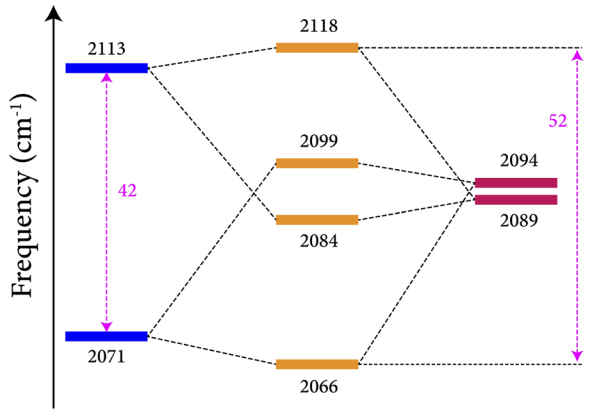

FIG. 5. Energy level diagrams indicating the energies in cm^{-1} of aromatic azides in the DMF solvent. Blue lines indicate the zeroth-order energy states of the azide asymmetric stretch modes, whereas dark pink lines describe the unperturbed vibrational states for combination bands. The orange lines represent the vibrational coupled states.

The zeroth-order energy states of the azide asymmetric stretch modes are at 2113 cm^{-1} and 2071 $cm^{-1,}$ corresponding to the first vibrationally excited state for unlabeled and labeled azides, respectively. The coupling strength is found to be 11.8 cm^{-1}. We have applied the same strategy to get the zeroth-order vibrational energy states and anharmonic coupling constants in H_2O and D_2O, as well, which are shown in Fig. S2 of the supplementary material. We have derived the coupling strength of H_2O and D_2O, which is 10.1 cm^{-1} and 9.9 cm^{-1}, respectively. However, in one of the earlier studies, Rodgers *et al.* have calculated the anharmonic coupling constants of –CO and –CN in various solvents using an analytical equation. Based on their result, they have concluded that the presence of Fermi resonance can reliably be used to determine the nature and strength of the hydrogen bonding for –CO and –CN infrared probes.[41] They have also inferred that the coupling constant obtained in the protic solvent should not exceed 7.7 cm^{-1}, and therefore, the H-bonding status can be evaluated from the calculated coupling constant.[41] However, in this study, using a methodology of matrix diagonalization with fewer assumptions, we find that the coupling constants are 11.8 cm^{-1} in DMF, 10.1 cm^{-1} in H_2O, and 9.9 cm^{-1} in D_2O, all exceeding 7.7 cm^{-1} regardless of the solvent. Therefore, this study demonstrates that the coupling constant causing the Fermi resonance in the aromatic azide does not have a sensitivity to the microscopic polarity and type of hydrogen bonding interaction.

On the other hand, the apparent switching of the spectral intensity of the high frequency and the low-frequency peak in the FT-IR of the aromatic azide after ^{15}N substitution can be explained in terms of the unperturbed first vibrational excited states calculated from the two-state model and Fermi resonance interaction. Before isotope labeling, the fundamental azide stretch vibration at 2113 cm^{-1} is higher in energy compared to the overtone or combination band at 2089 cm^{-1}. This scenario gets changed for the labeled azide as the fundamental band is more strongly perturbed due to the reduced mass effect compared to the overtone or combination band. As a result, the fundamental band underwent a large red-shift and ended up being lower in energy to the overtone or combination band. It can be inferred from the present study that if the shoulder peak in the FT-IR spectra corresponding to the Fermi resonance appears at a higher frequency than the main peak, the Fermi resonance can be easily decoupled by the isotope substitution. However, when the Fermi resonance band comes at a lower frequency than the main peak, the isotope substitution may not be an excellent strategy to decouple the participating vibrations in the Fermi resonance. In summary, this study demonstrates that the elimination of the Fermi resonance with single isotope labeling is inadequate in the aromatic azide systems. Therefore, multiple isotope substitution of nitrogen atoms in the azide probe would be required to decouple the Fermi resonance completely.

E. Quantum chemical calculation

1. Fermi resonance enhances the spectral shift

To understand the origin of the unexpectedly large peak shift of the azide asymmetric stretch in the FT-IR of the aromatic azide due to isotope substitution, we have calculated harmonic frequencies using the B3LYP/6-311++G level of theory coupled with a CPCM solvation model for DMF. The unlabeled and ^{15}N labeled methyl azide, cyclohexyl azide, and phenyl azide molecule have been compared. The values of the frequencies and the corresponding frequency shifts are tabulated in Table S3 of the supplementary material. Interestingly, it can be observed that the frequency shift of the azide is ~44 cm^{-1} due to isotope labeling, which is found to be independent of the molecular structure, whether it is attached to the aromatic group or aliphatic group. This result suggests that the unexpectedly large frequency shift (52 cm^{-1}) of the aromatic azide due to isotope labeling is exclusively due to the Fermi resonance and not from the resonance effect of the aromatic ring itself.

2. Anharmonic frequency analysis

The anharmonic frequency analysis has been performed for both unlabeled and labeled aromatic azides using the Gaussian 16 package to find out the origin of the Fermi resonance band. Another objective of the anharmonic frequency analysis is to unveil the molecular origin behind the ineffectiveness of the isotope labeling strategy in removing the Fermi resonance band in the case of aromatic azide. The anharmonic calculation has been performed at the B3LYP/6-311+G** level of theory using the CPCM solvation model for DMF. The harmonic and anharmonic frequencies of the azide asymmetric stretch of the unsubstituted azide are found to be 2216.1 cm^{-1} and 2175.7 cm^{-1}, whereas 2170.1 cm^{-1} and 2124.0 cm^{-1} for substituted azides, respectively (mode 79, Tables S4 and S5 of the supplementary material).

Based on the threshold of the Fermi resonance described in detail in Sec. II B, in the quantum chemical calculation part we have tabulated all those near-resonant combination modes that can participate in the Fermi resonance with the azide asymmetric stretch. We have also listed the difference in the frequency of those bands from the azide stretch, the respective cubic interaction force constant (k_{ijk}), and the difference of second-order perturbative energy to the variational energy in Table III. In comparison to the earlier

TABLE III. List of possible combination bands of unlabeled and labeled aromatic azides that can participate in the Fermi resonance with the azide asymmetric stretch (mode 79). The interactions associated with the frequency difference of maximum ±25.0 cm^{-1} from the azide asymmetric stretch, the minimum of cubic interaction force constant 1 cm^{-1}, and the minimum difference of the second-order perturbative energy (PT2) to the variational energy of more than 1 cm^{-1} are listed as Fermi resonance interaction. All the three parameters are in cm^{-1}.

I	J + K		Freq. diff.	Cubic int. force. const. (k_{ijk})	PT2-variat. diff.
			Unlabeled		
79	63	38	9.7	36.9	32.1
	63	39	0.8	−7.2	76.1
			^{15}N labeled		
79	63	35	24.2	−46.0	5.0
	59	38	1.5	4.4	1.8

anharmonic analysis of 4-azido-L-phenylalanine, which reveals several combination bands participating in the Fermi resonance with the azide asymmetric stretch,[40] the unsubstituted azide in this study shows only two combination bands, which can participate in the Fermi resonance (Table III). A less number of available combination bands thus uncover why the aromatic azide shows less asymmetric FT-IR spectra and less complex 2D-IR signals compared to 4-azido-L-phenylalanine in the earlier study.[40] In Fig. 6, we have shown the normal modes from the most suited combination band in each case of the azides to take part in the Fermi resonance along with the corresponding azide asymmetric stretch. However, all the normal modes for both the cases, which mainly consist of the N_3 symmetric stretch, C–N stretch, phenyl ring vibration, phenyl C–H in-plane and out of plane bending, CH_2 twisting, and so on, are described in great detail in Tables S4 and S5 and Figs. S4 and S5 in the supplementary material. We have also shown the atomic displacement vector (light blue) associated with the molecular vibration of these normal modes in Figs. S4 and S5 for better visualization.

The two combination bands for unlabeled azides consist of modes 38 (844.9 cm^{-1}) and 63 (1361.5 cm^{-1}) and modes 39 (853.8 cm^{-1}) and 63 with the corresponding k_{ijk} values of 36.9 cm^{-1} and −7.2 cm^{-1}, respectively (Tables III and S4, and Fig. S4 of the supplementary material). Interestingly, the normal mode 63 is involved in both the combination bands, which can take part in the Fermi resonance interaction with the azide asymmetric stretch (mode 79). Mode 63 consists of mainly the N_3 symmetric stretch, C–N stretch, phenyl ring vibration, and phenyl C–H bend. Additionally, mode 38 of the first combination band also consists of a weakly coupled azide bend. Therefore, α-N of the azide is spatially overlapped with both the transitions participating in the Fermi resonance. These combination bands, which are strongly coupled with α-N of the azide group, are being modulated similarly to that of the azide asymmetric stretch due to ^{15}N labeling, which explains why ^{15}N substitution has little effect in decoupling these modes from the azide asymmetric stretch.

The anharmonic frequency analysis of the labeled azide shows that there are two combination bands as well, like that of the unlabeled azide. These combination bands consist of modes 35 (785.2 cm^{-1}) and 63 (1360.7 cm^{-1}) and modes 38 (844.0 cm^{-1}) and 59 (1324.6 cm^{-1}), respectively, which can participate in the Fermi

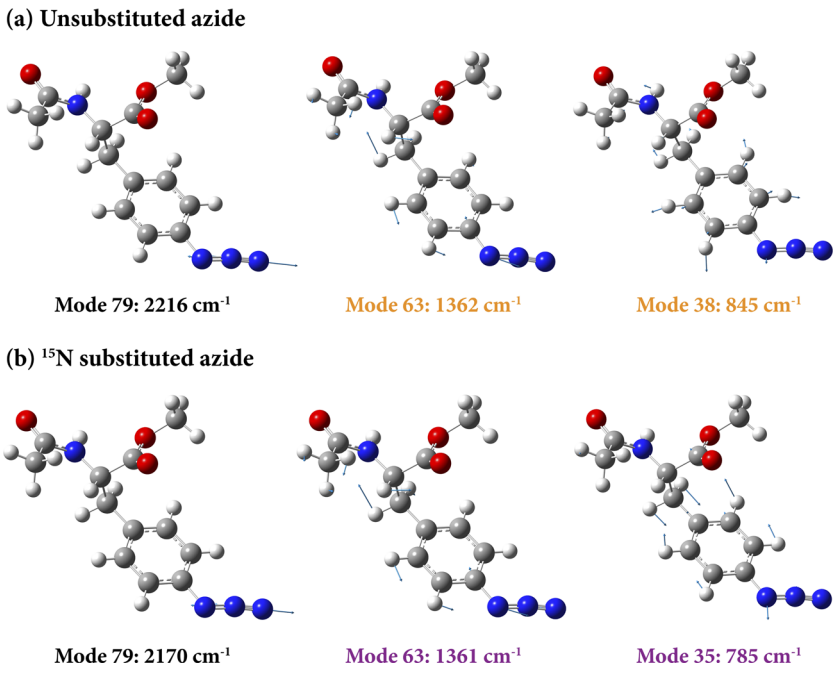

FIG. 6. Molecular picture of the azide asymmetric stretch mode and the normal modes of the most suited combination band to take part in the Fermi resonance with the azide asymmetric stretch mode 79 based on the maximum cubic interaction force constant in the case of (a) unlabeled and (b) labeled azides along with their corresponding harmonic frequencies calculated at the B3LYP/6-311+G** level of theory. The displacement vector is shown in light blue color for all the modes. Modes 63 and 38 in (a) and 63 and 35 in (b) that can participate in the Fermi resonance involve the N atom of the azide group.

resonance with the azide asymmetric stretch (Table S5 and Fig. S5 of the supplementary material). Among these two, the Fermi resonance interaction of the azide asymmetric stretch with the combination band consisting of modes 35 and 63 is the most suited due to the large k_{ijk} of −46.0 compared to 4.4 of the other band (Table III). Furthermore, as the normal mode, 63 consists of phenyl ring vibration, which strongly coupled with the N_3 symmetric stretch and C–N stretch remains unaffected due to isotope labeling. The normal mode 63 gets red-shifted only by 0.8 cm^{-1} though there is a significant red-shift of ~52.0 cm^{-1} in the azide asymmetric stretch band. Therefore, mode 63 plays a pivotal role in both the unlabeled and labeled azides in constructing different combination band with other normal modes to participate in the Fermi resonance with the azide asymmetric stretch. Additionally, it can also be observed that normal modes 35 and 38 of the combination band also involve the first N atom of the azide group. Therefore, it can be concluded from this anharmonic analysis that isotope substitution does not impact these combination bands significantly. Hence, one of the key strategies to remove the Fermi resonance would be to disrupt mode 63 to completely decouple phenyl ring vibration from that of the N_3 symmetric stretch and C–N stretch where the α-N atom is shared between two transitions participating in the Fermi resonance. Thus, the most promising approach might be to simultaneously label both α and β N atoms of the azide group, which may lead to the complete removal of the Fermi resonance band in the case of the aromatic azide.

IV. CONCLUSION

The effect of isotope substitution on the middle N atom of the azide group in 4-azido-L-phenylalanine has been investigated to understand how it affects the vibrational properties and relaxation dynamics of the azido stretching mode, a promising IR probe. It is observed that the steady-state FT-IR spectra show a complex absorption spectrum corresponding to the azide asymmetric stretch vibration accompanied with a shoulder peak, arising due to the Fermi resonance between the azide asymmetric stretch and the near-resonant combination bands. Upon isotope substitution, the asymmetric stretch of the aromatic azide undergoes a large red-shift but, unfortunately, not enough to decouple the participating modes in the Fermi resonance. The anharmonic coupling constants corresponding to the Fermi resonance transitions for H_2O, D_2O, and DMF calculated using the two-state model are all above 7.7 cm^{-1}, which suggests that the aromatic azide band is not particularly sensitive to the local hydrogen bonding environment. To investigate the effect of the isotope labeling on the population relaxation dynamics, we carried out the ultrafast pump-probe experiment in DMF. It is observed that both the unlabeled and labeled azides show a damped oscillatory decay, which is assigned to the coherent dynamics of the Fermi coupled states. The period of damped oscillation is also observed to be consistent with the frequency gap between the two vibrational states that participate in the Fermi resonance. Our results show that the effect of isotope labeling on vibrational lifetimes is not so significant contrary to the earlier report where researchers have shown a drastic increase in the lifetime upon isotope substitution.

To uncover the origin of the Fermi resonances in both cases, we performed the anharmonic frequency analysis. The anharmonic vibrational analysis shows that there are two combination bands in each case of the unlabeled and labeled azides, which can participate in the Fermi resonance with the azide asymmetric stretch mode. It also unveils that some of the normal modes of those combination bands involve one of the N (α-N) atoms of the azide group. As a result, it is shared between two transitions participating in the Fermi resonance. Therefore, isotope substitution has little impact on these combination bands to take part in the Fermi resonance effectively. In a nutshell, this study unravels that the method of incorporating a heavy isotope in the infrared probe does not guarantee the removal of the Fermi resonance despite the significant spectral shift of the azide asymmetric stretch. When the Fermi resonance peak appears at a higher frequency than that of the main azide asymmetric stretch, there is a higher chance that the isotope labeling would be successful in eliminating the Fermi resonance. Based on the anharmonic analysis, a promising alternative to eliminate the Fermi resonance would be to simultaneously label multiple atomic centers (α and β N) of the azide probe with ^{15}N isotopes. Hence, more research is required based on similar approaches to developing a highly sensitive infrared probe based on the aromatic azide having longer vibrational lifetime and site-specificity to study protein dynamics.

SUPPLEMENTARY MATERIAL

See the supplementary material for the detailed description of the material synthesis, two-state model of the aromatic azide in H_2O and D_2O, comparison of different fitting model for the pump-probe decay, quantum chemical calculation, and diagonal slice of the 2D-IR spectrum.

AUTHORS' CONTRIBUTIONS

J.Y.P. and S.M. contributed equally to this work. H.H., K.K., and M.C. contributed to conceptualization and methodology; J.Y.P., S.M., and H.-J.K. helped in validation; J.Y.P., S.M., and K.K. conducted the formal analysis; J.Y.P. conducted the investigation; H.-J.K. and H.H. conducted the synthesis; J.Y.P. and S.M. helped in data curation; S.M. helped in writing the original draft; S.M., J.Y.P., P.K.S., and K.K. reviewed and edited the manuscript; J.Y.P., S.M., and K.K. helped in visualization; M.C. helped in supervision; M.C. helped in project administration; H.H. and M.C. helped in funding acquisition.

ACKNOWLEDGMENTS

This work was supported by the Institute for Basic Science (Grant No. IBSR023-D1). H.H. is grateful for the financial support from the National Research Foundation (NRF) of Korea funded by the Ministry of Science and ICT (Grant No. NRF2020R1F1A1049520).

The authors declare no conflicts of interest.

DATA AVAILABILITY

The data that support the findings of this study are available from the corresponding author upon reasonable request.

REFERENCES

[1] R. Adhikary, J. Zimmermann, and F. E. Romesberg, Chem. Rev. **117**, 1927 (2017).
[2] J. Zimmermann, M. C. Thielges, Y. J. Seo, P. E. Dawson, and F. E. Romesberg, Angew. Chem., Int. Ed. **50**, 8333 (2011).
[3] M. M. Waegele, R. M. Culik, and F. Gai, J. Phys. Chem. Lett. **2**, 2598 (2011).
[4] J.-H. Choi, D. Raleigh, and M. Cho, J. Phys. Chem. Lett. **2**, 2158 (2011).
[5] S. Ye, E. Zaitseva, G. Caltabiano, G. F. X. Schertler, T. P. Sakmar, X. Deupi, and R. Vogel, Nature **464**, 1386 (2010).
[6] D. C. Urbanek, D. Y. Vorobyev, A. L. Serrano, F. Gai, and R. M. Hochstrasser, J. Phys. Chem. Lett. **1**, 3311 (2010).
[7] H. Taskent-Sezgin, J. Chung, P. S. Banerjee, S. Nagarajan, R. B. Dyer, I. Carrico, and D. P. Raleigh, Angew. Chem., Int. Ed. **49**, 7473 (2010).
[8] M. Maj, C. Ahn, B. Błasiak, K. Kwak, H. Han, and M. Cho, J. Phys. Chem. B **120**, 10167 (2016).
[9] M. Okuda, K. Ohta, and K. Tominaga, J. Chem. Phys. **142**, 212418 (2015).
[10] M. Maj, C. Ahn, D. Kossowska, K. Park, K. Kwak, H. Han, and M. Cho, Phys. Chem. Chem. Phys. **17**, 11770 (2015).
[11] R. Adhikary, J. Zimmermann, P. E. Dawson, and F. E. Romesberg, ChemPhysChem **15**, 849 (2014).
[12] C. G. Bazewicz, M. T. Liskov, K. J. Hines, and S. H. Brewer, J. Phys. Chem. B **117**, 8987 (2013).
[13] K.-K. Lee, K.-H. Park, C. Joo, H.-J. Kwon, J. Jeon, H.-I. Jung, S. Park, H. Han, and M. Cho, J. Phys. Chem. B **116**, 5097 (2012).
[14] A. Ghosh, J. S. Ostrander, and M. T. Zanni, Chem. Rev. **117**, 10726 (2017).
[15] A. L. Le Sueur, R. E. Horness, and M. C. Thielges, Analyst **140**, 4336 (2015).
[16] M. Grechko and M. T. Zanni, J. Chem. Phys. **137**, 184202 (2012).
[17] H. Bian, W. Zhao, and J. Zheng, J. Chem. Phys. **131**, 124501 (2009).
[18] C. Fang, J. D. Bauman, K. Das, A. Remorino, E. Arnold, and R. M. Hochstrasser, Proc. Natl. Acad. Sci. U. S. A. **105**, 1472 (2008).
[19] S. Park, K. Kwak, and M. D. Fayer, Laser Phys. Lett. **4**, 704 (2007).
[20] H. Maekawa, C. Toniolo, A. Moretto, Q. B. Broxterman, and N.-H. Ge, J. Phys. Chem. B **110**, 5834 (2006).
[21] J. Edler and P. Hamm, J. Chem. Phys. **119**, 2709 (2003).
[22] K.-K. Lee, K.-H. Park, C. Joo, H.-J. Kwon, H. Han, J.-H. Ha, S. Park, and M. Cho, Chem. Phys. **396**, 23 (2012).
[23] R. Bloem, K. Koziol, S. A. Waldauer, B. Buchli, R. Walser, B. Samatanga, I. Jelesarov, and P. Hamm, J. Phys. Chem. B **116**, 13705 (2012).
[24] M. J. Tucker, X. S. Gai, E. E. Fenlon, S. H. Brewer, and R. M. Hochstrasser, Phys. Chem. Chem. Phys. **13**, 2237 (2011).
[25] M. W. Nydegger, S. Dutta, and C. M. Cheatum, J. Chem. Phys. **133**, 134506 (2010).
[26] S. Ramos, K. J. Scott, R. E. Horness, A. L. Le Sueur, and M. C. Thielges, Phys. Chem. Chem. Phys. **19**, 10081 (2017).
[27] J. M. Rodgers, W. Zhang, C. G. Bazewicz, J. Chen, S. H. Brewer, and F. Gai, J. Phys. Chem. Lett. **7**, 1281 (2016).
[28] D. E. Levin, A. J. Schmitz, S. M. Hines, K. J. Hines, M. J. Tucker, S. H. Brewer, and E. E. Fenlon, RSC Adv. **6**, 36231 (2016).
[29] C. G. Bazewicz, J. S. Lipkin, E. E. Smith, M. T. Liskov, and S. H. Brewer, J. Phys. Chem. B **116**, 10824 (2012).
[30] J. S. Lipkin, R. Song, E. E. Fenlon, and S. H. Brewer, J. Phys. Chem. Lett. **2**, 1672 (2011).
[31] S. H. Brewer, B. Song, D. P. Raleigh, and R. B. Dyer, Biochemistry **46**, 3279 (2007).
[32] S. M. Decatur, Acc. Chem. Res. **39**, 169 (2006).
[33] Z. Getahun, C.-Y. Huang, T. Wang, B. De León, W. F. DeGrado, and F. Gai, J. Am. Chem. Soc. **125**, 405 (2003).
[34] M. P. Wolfshorndl, R. Baskin, I. Dhawan, and C. H. Londergan, J. Phys. Chem. B **116**, 1172 (2012).
[35] K.-I. Oh, J.-H. Lee, C. Joo, H. Han, and M. Cho, J. Phys. Chem. B **112**, 10352 (2008).
[36] A. T. Krummel and M. T. Zanni, J. Phys. Chem. B **112**, 1336 (2008).
[37] Z. Ganim, H. S. Chung, A. W. Smith, L. P. DeFlores, K. C. Jones, and A. Tokmakoff, Acc. Chem. Res. **41**, 432 (2008).
[38] J.-H. Choi, K.-I. Oh, and M. Cho, J. Chem. Phys. **129**, 174512 (2008).
[39] E. S. Park and S. G. Boxer, J. Phys. Chem. B **106**, 5800 (2002).
[40] J. Zhang, L. Wang, J. Zhang, J. Zhu, X. Pan, Z. Cui, J. Wang, W. Fang, and Y. Li, J. Phys. Chem. B **122**, 8122 (2018).
[41] J. M. Rodgers, R. M. Abaskharon, B. Ding, J. Chen, W. Zhang, and F. Gai, Phys. Chem. Chem. Phys. **19**, 16144 (2017).
[42] Y. Kwon, C. Lee, and S. Park, Chem. Phys. **445**, 38 (2014).
[43] J. F. Bertran, L. Ballester, L. Dobrihalova, N. Sánchez, and R. Arrieta, Spectrochim. Acta, Part A **24**, 1765 (1968).
[44] K.-H. Park, J. Jeon, Y. Park, S. Lee, H.-J. Kwon, C. Joo, S. Park, H. Han, and M. Cho, J. Phys. Chem. Lett. **4**, 2105 (2013).
[45] H. Bian, J. Li, X. Wen, and J. Zheng, J. Chem. Phys. **132**, 184505 (2010).
[46] A. L. Le Sueur, S. Ramos, J. D. Ellefsen, S. Cook, and M. C. Thielges, Anal. Chem. **89**, 5254 (2017).
[47] J. S. Italia, C. Latour, C. J. J. Wrobel, and A. Chatterjee, Cell Chem. Biol. **25**, 1304 (2018).
[48] A. Creon, I. Josts, S. Niebling, N. Huse, and H. Tidow, Struct. Dyn. **5**, 064701 (2018).
[49] E. M. Tookmanian, E. E. Fenlon, and S. H. Brewer, RSC Adv. **5**, 1274 (2015).
[50] N. Shao, N. S. Singh, S. E. Slade, A. M. E. Jones, and M. K. Balasubramanian, Sci. Rep. **5**, 17196 (2015).
[51] W. Wang, T. Li, K. Felsovalyi, C. Chen, T. Cardozo, and M. Krogsgaard, ACS Chem. Biol. **9**, 2165 (2014).
[52] J. W. Chin, S. W. Santoro, A. B. Martin, D. S. King, L. Wang, and P. G. Schultz, J. Am. Chem. Soc. **124**, 9026 (2002).
[53] L. Shi, X. Liu, L. Shi, H. T. Stinson, J. Rowlette, L. J. Kahl, C. R. Evans, C. Zheng, L. E. P. Dietrich, and W. Min, Nat. Methods **17**, 844–851 (2020).
[54] M. J. Frisch, G. W. Trucks, H. B. Schlegel, G. E. Scuseria, M. A. Robb, J. R. Cheeseman, G. Scalmani, V. Barone, G. A. Petersson, H. Nakatsuji, X. Li, M. Caricato, A. V. Marenich, J. Bloino, B. G. Janesko, R. Gomperts, B. Mennucci, H. P. Hratchian, J. V. Ortiz, A. F. Izmaylov, J. L. Sonnenberg, D. Williams-Young, F. Ding, F. Lipparini, F. Egidi, J. Goings, B. Peng, A. Petrone, T. Henderson, D. Ranasinghe, V. G. Zakrzewski, J. Gao, N. Rega, G. Zheng, W. Liang, M. Hada, M. Ehara, K. Toyota, R. Fukuda, J. Hasegawa, M. Ishida, T. Nakajima, Y. Honda, O. Kitao, H. Nakai, T. Vreven, K. Throssell, J. A. Montgomery, Jr., J. E. Peralta, F. Ogliaro, M. J. Bearpark, J. J. Heyd, E. N. Brothers, K. N. Kudin, V. N. Staroverov, T. A. Keith, R. Kobayashi, J. Normand, K. Raghavachari, A. P. Rendell, J. C. Burant, S. S. Iyengar, J. Tomasi, M. Cossi, J. M. Millam, M. Klene, C. Adamo, R. Cammi, J. W. Ochterski, R. L. Martin, K. Morokuma, O. Farkas, J. B. Foresman, and D. J. Fox, GAUSSIAN 16 Revision B.01, Gaussian, Inc., Wallingford, CT, 2016.
[55] J. B. Foresman and Æ. Frisch, *Exploring Chemistry with Electronic Structure Methods*, 3rd ed. (Gaussian, Inc., Wallingford, CT, 2015).